Lawrence Berkeley National Laboratory
Recent Work

Title
Observation of chiral phonons.

Permalink

Journal

ISSN

Authors
Zhu, Hanyu
Yi, Jun
Li, Ming-Yang
et al.

Publication Date

DOI

Peer reviewed

Title: Observation of chiral phonons

Authors: Hanyu Zhu[1,2], Jun Yi[1], Ming-Yang Li[3], Jun Xiao[1], Lifa Zhang[4], Chih-Wen Yang[3], Robert A. Kaindl[2], Lain-Jong Li[3], Yuan Wang[1,2]* and Xiang Zhang[1,2]*

Affiliations:

[1]Nanoscale Science and Engineering Center (NSEC), University of California, Berkeley, CA 94720, USA.

[2]Materials Sciences Division, Lawrence Berkeley National Laboratory, Berkeley, CA 94720, USA.

[3]Physical Sciences and Engineering Division, King Abdullah University of Science and Technology, Thuwal, 23955-6900, Kingdom of Saudi Arabia.

[4]Department of Physics, Nanjing Normal University, Nanjing, Jiangsu 210023, China.

*Correspondence to: xzhang@me.berkeley.edu and yuanwang@berkeley.edu

Abstract: Chirality reveals symmetry breaking of the fundamental interaction of elementary particles. In condensed matter, for example, the chirality of electrons governs many unconventional transport phenomena such as the quantum Hall effect. Here, we show that phonons can exhibit intrinsic chirality in monolayer tungsten diselenide (WSe_2). The broken inversion symmetry of the lattice lifts the degeneracy of clockwise and counter-clockwise phonon modes at the corners of the Brillouin zone. We identified the phonons by the intervalley transfer of holes through hole-phonon interactions during the indirect infrared absorption, and confirmed their chirality by the infrared circular dichroism arising from pseudo-angular momentum conservation. The chiral phonons are important for electron-phonon coupling in solids, phonon-driven topological states and energy-efficient information processing.

One Sentence Summary: Circularly rotating chiral phonons are observed in monolayer WSe_2.

Main Text:

Chirality is a fundamental property of an object not identical to its mirror image. For elementary and quasi-particles, it is an important quantum concept at the heart of modern physics. For example, the discovered handedness of neutrinos in electroweak interaction revolutionized our understanding of the universal parity conservation law. Chiral Fermions with spin-momentum locking can emerge in solid state systems, such as the recently observed Weyl semimetals with inversion-symmetry-breaking lattices (*1*). Electron chirality in graphene defined through pseudospin was found to cause unique transport properties like unconventional Landau quantization and Klein tunneling (*2*, *3*). Meanwhile, electrons in monolayer transition metal dichalcogenides with broken inversion symmetry display optical helicity which opens the new field of valleytronics (*4*). The outstanding question is whether bosonic collective excitations such

as phonons can attain chirality. Recently, the intrinsic chirality of phonons without applied external magnetic fields in an atomic lattice was predicted theoretically at the corners of the Brillouin zone of an asymmetric two-dimensional hexagonal lattice (5). Because of the three-fold rotational symmetry of the crystal and the momentum vectors, the vibrational plane wave is comprised of unidirectional atomic circular rotation. Since the phonons in the same valley have distinct energy levels, the rotation is not the superposition of linear modes, in contrast to the circular polarization in non-chiral media (6). The hypothetical chiral phonons are potentially important for the control of intervalley scattering (7, 8), lattice-modulation-driven electronic phase transitions (9, 10) and topological states (11), as well as information carriers that can be robust against decoherence for solid state quantum information applications (12).

Here, we report the observation of intrinsic chiral phonons using transient infrared spectroscopy in the atomic lattice of monolayer WSe_2. A particle's angular momentum is calculated by the phase change under a rotational transformation. This definition can be extended for quasi-particles in solid lattices with discrete spatial symmetry, as long as the rotation is in the crystalline symmetry group (13). For inversion-symmetry-breaking 2D hexagonal lattice like monolayer WSe_2 (Fig. 1A), phonons with well-defined pseudo-angular momentum (PAM) are located at Γ, K and K' points in the reciprocal space (5). Because they inherit the three-fold rotational (C_3) symmetry of the lattice, their function of motion must be C_3 invariant except for a phase difference, i.e. circular (14). The K and K' phonons are particularly interesting because there is no reflection line that preserves both the lattice and their momentum (Fig. S5). Therefore, the atomic rotation cannot be reversed without changing its momentum or energy. For example, if we attempt to reverse the rotational direction of the Se atoms in longitudinal optical phonon LO(K) while keeping the relative phase determined by the $q = K$ momentum, the mode changes to a longitudinal acoustic phonon LA(K) that oscillates at a different frequency. It means that unlike the Γ phonon, such a rotation cannot be decomposed into orthogonal linear vibrations with $\pm\pi/2$ phase shift. On the other hand, in order to maintain the same mode, the relative phase must be reversed, resulting in a phonon at the K' point.

We deduce the phonon PAM l for each mode from the phase change after counter-clockwise 120° rotation: $\hat{C}_3(u_k) = e^{-i(2\pi/3)l}u_k$, where u_k is the function of atomic motion (Fig. S6). Since LA(K) is always C_3 symmetric, it has $l = 0$, while LO(K) gains negative phase after rotation (becomes ahead of time) and thus $l = 1$. The K phonons with different PAM are completely non-degenerate due to the mass difference between W and Se. The lifting of degeneracy guarantees that each mode has a distinctive selection rule for the electron-phonon and optical scattering (Table S1). These features differentiate the intrinsically chiral phonons from any previously investigated phonons where circular atomic motion results from superposing linear polarized eigenmodes (6, 15, 16). Chirality in the absence of an external magnetic flux is also distinguished from the magnetic-field-induced split of degenerate superposition modes (17). Finally, both the physical origin and properties of the atomic chiral phonons are fundamentally different from previous phononic-crystal-based chirality from geometric engineering or topological edge states (18–20).

The chiral phonon is identified by its scattering with holes using an optical pump-probe technique (Fig. 1B and Fig. S2). The linear momentum, PAM and energy of the respective phonon modes are determined by characterizing all the other particles involved in the intervalence band transition (IVBT) process (14). First, we inject holes at the K valley by a left-circular-polarized (LCP) optical pump pulse. The K-valley-polarized hole relaxes to the valence

band edge with initial linear momentum $p_i = -K$. It can transit to the K' point ($p_f = K$) by emitting a K phonon ($q = p_i - p_f = -2K = K$), but the intermediate state is virtual because the spin-conserving state has much higher energy due to large spin-orbit coupling. Then we send an infrared pulse to satisfy the energy conservation and place the hole in the spin-split band at K'. Since the hole states have zero PAM, the PAM of the phonon must be equal to the spin angular momentum of the absorbed infrared photon. Therefore, the LCP pulse controls the creation of only LO(K) phonons. Eventually, we recognize the final spin-split state in the opposite valley by the energy and RCP polarization of its radiative decay. The selection rule of phonon creation will be identical if the hole first absorbs an IR photon, transits to an intermediate state within the valley, and then emits a phonon, as long as the final state is the same. The phonon annihilation is negligible because the population is very low as the sample temperature is kept at 82 K, lower than the Debye temperature of all phonon modes at the K or K' points. The selection is also not affected by a small momentum distribution of the initial and final holes (*14*) due to finite thermal energy or the strong many-body interaction (*21*). This is because like the optical valley-selectivity, the contrast of electron-phonon coupling strength remains large in the vicinity of K and K' even if the PAM is only defined on these points.

To determine the linear momentum of the involved phonon, we measure the linear momentum of the initial and final holes. Under circularly-polarized pump excitation, the majority of holes maintain their linear momentum near the original valley as shown by the positive helicity of the photoluminescence. The final linear momentum of the spin-split states is read out by the polarization of their luminescence at higher energy than the original pump photon (Fig. 2A). We measure the difference of luminescence with the same polarization as the pump light (I_{same}) and the opposite polarization (I_{oppo}) as a function of the probe delay time τ (Fig. 2B). We find the polarized luminescence ($I_{same} - I_{oppo}$) is positive for $\tau < 0.2$ ps, indicating that the spin-flipping intravalley IVBT has a higher probability when the IR probe arrives immediately after the excitation of holes. This is because spin is not strictly conserved for optical transitions away from the high symmetry points. However, the process is forbidden at the valley center with incident light perpendicular to the lattice plane, so its magnitude decays with a lifetime of 0.2 ps as the non-equilibrium carriers thermalize to the band edge (*22, 23*). After that, the luminescence switches polarization as a result of the dominant spin-conserving intervalley IVBT. It shows that the majority of final holes have a linear momentum opposite to the initial holes. The momentum must have been transferred to phonons instead of defects, as seen from the order-of-magnitude weaker defect-assisted one-phonon Raman scattering compared with the two-phonon process (Fig. S7). Directional intervalley transfer through electron-electron interactions (*24*) is excluded because the pump is not in resonance with the A-exciton, and the signal is linearly proportional to the hole density (Fig. S8). The exchange interaction reduces the polarization of the holes but should not create an opposite polarization (*25*). Finally, the depolarization plus the decay of the hole population yields a joint lifetime of about 2 ps for the polarized luminescence, which agrees with previous exciton studies (*26*). To further verify the nature of the final holes, we measure the polarized luminescence at different collection energy with $\tau = 0.8$ ps. The emission spectra obtained with different IR photon energy are all close to the B-exciton photoluminescence (Fig. 2C, Fig. S12). It proves that the emission is the radiative decay of a real state near the edge of the spin-split band, instead of a virtual state. Therefore, we use the luminescence from 2.05 to 2.19 eV to quantify the indirect infrared absorption and the phonon creation.

The PAM of valley phonons is determined by measuring the polarization selection of the absorbed IR photon, resulting from the chiral electron-phonon interaction. With LCP excitation,

the intervalley transition of holes from the K valley can either absorb an LCP IR photon to produce LO phonons, or absorb an RCP IR photon to produce TA/A_1 phonons (Fig. 3A). We observe different IR absorption when the probe has the same polarization as the pump light (α_{same}), and that for the opposite polarization (α_{oppo}). This infrared circular dichroism (CD = α_{same} − α_{oppo}) demonstrates that scattering cross-sections of the two processes are indeed not equal, due to the difference of electron-phonon coupling strength. As shown in Fig.3B, the CD at 82 K is always positive for valley-polarized holes. Since the holes have zero PAM regardless of valley index or spin-split bands, the angular momentum of the IR photon is either transferred to the spin or phonon. The initial intravalley IVBT gives positive CD because the electronic spin flips from -1/2 in the spin-split band to +1/2 at the valence band edge at the K point. However, this contribution decays fast as a function of IR delay in accordance to Fig. 2B. Thus, the intervalley phonon-creating transition is the dominant source of positive CD for $\tau \geq 0.8$ ps. It indicates that the LO branch contributes most to the indirect IR absorption. For non-chiral systems, although photons with opposite circular polarization may interact with different particles, the probabilities are always equal. Therefore, the CD is the signature of intrinsic phonon chirality.

The energy of this phonon mode is measured according to energy conservation: the energy sum of the incoming particles, the infrared photon and the initial holes must be equal to that of the outgoing particles, the chiral phonon and the final holes (*14*). We observe that the CD spectrum at $\tau = 0.8$ ps (Fig. 3C) is a step function with a clear threshold near 0.448±0.002 eV, broadened by the spectral width of the IR pulse. The shape corresponds to a transition from a hole at the valence edge to a band with parabolic dispersion in two dimensions (Fig. S9). This value is distinguished from either the intra-excitonic transition (*27*) or the exciton dissociation energy (*21*). Next, we find the ground state configuration of the initial holes is the dark A-trion at 1.671±0.006eV (Fig. S11) (*28*) based on the dominant bright A-trion photoluminescence (Fig. S1). We verify that the dark trions are near thermal equilibrium, because the IR spectrum is very different from non-equilibrium carriers with excessive energy at $\tau = 0$ ps (Fig. S10). The final state is the bright B-trion at 2.090±0.005 eV measured through its emission (Fig. S12). Summarizing these values, we deduce the phonon energy $E_{\text{phonon}} = E_{\text{photon}} + E_{\text{i}} − E_{\text{f}} = 29±8$ meV, which agrees with the first-principles calculation and the Raman spectrum for the LO(K) mode (Fig. S7 and S9). The uncertainty may be reduced in the future by improving the uniformity of the sample and the spectral resolution of the B-exciton emission. Better spectroscopy will also potentially reveal details about the chiral phonon-exciton coupling that are not resolvable with the current signal-to-noise ratio, such as the contribution from LA phonons and the various pathways of the indirect transition.

Our findings of chiral phonons are fundamentally important for potential experimental tests of quantum theories with chiral bosons (*29*) in the solid state. It also provides a possible route for controlling valley and spin through electron-phonon scattering and strong spin-phonon interactions (*16*). Furthermore, the lifting of degeneracy by chirality offers robust PAM information against decoherence and long-range perturbation, and offers a new degree of freedom to the design and implementation of phononic circuitry (*30*) at the atomic scale without magnetic fields.

References and Notes:

1. M. Z. Hasan, S.-Y. Xu, I. Belopolski, S.-M. Huang, Discovery of Weyl Fermion Semimetals and Topological Fermi Arc States. *Annu. Rev. Condens. Matter Phys.* **8**, 289–309 (2017).

2.   F. D. M. Haldane, Model for a Quantum Hall Effect without Landau Levels: Condensed-Matter Realization of the "Parity Anomaly." *Phys. Rev. Lett.* **61**, 2015–2018 (1988).

3.   S. Das Sarma, S. Adam, E. H. Hwang, E. Rossi, Electronic transport in two-dimensional graphene. *Rev. Mod. Phys.* **83**, 407–470 (2011).

4.   J. R. Schaibley *et al.*, Valleytronics in 2D materials. *Nat. Rev. Mater.* **1**, 16055 (2016).

5.   L. Zhang, Q. Niu, Chiral Phonons at High-Symmetry Points in Monolayer Hexagonal Lattices. *Phys. Rev. Lett.* **115**, 115502 (2015).

6.   H. Katsuki *et al.*, All-optical control and visualization of ultrafast two-dimensional atomic motions in a single crystal of bismuth. *Nat. Commun.* **4**, ncomms3801 (2013).

7.   H. Zeng, J. Dai, W. Yao, D. Xiao, X. Cui, Valley polarization in MoS2 monolayers by optical pumping. *Nat. Nanotechnol.* **7**, 490–493 (2012).

8.   B. R. Carvalho *et al.*, Intervalley scattering by acoustic phonons in two-dimensional MoS$_2$ revealed by double-resonance Raman spectroscopy. *Nat. Commun.* **8**, ncomms14670 (2017).

9.   M. Rini *et al.*, Control of the electronic phase of a manganite by mode-selective vibrational excitation. *Nature*. **449**, 72–74 (2007).

10. M. Först, R. Mankowsky, A. Cavalleri, Mode-Selective Control of the Crystal Lattice. *Acc. Chem. Res.* **48**, 380–387 (2015).

11. G. Jotzu *et al.*, Experimental realization of the topological Haldane model with ultracold fermions. *Nature*. **515**, 237–240 (2014).

12. K. C. Lee *et al.*, Entangling Macroscopic Diamonds at Room Temperature. *Science*. **334**, 1253–1256 (2011).

13. R. C. Johnson, Angular momentum on a lattice. *Phys. Lett. B*. **114**, 147–151 (1982).

14. Materials, methods and additional information are available in the supplementary materials.

15. S.-Y. Chen, C. Zheng, M. S. Fuhrer, J. Yan, Helicity-Resolved Raman Scattering of MoS2, MoSe2, WS2, and WSe2 Atomic Layers. *Nano Lett.* **15**, 2526–2532 (2015).

16. T. F. Nova *et al.*, An effective magnetic field from optically driven phonons. *Nat. Phys.* **13**, 132 (2017).

17. G. Schaack, Observation of circularly polarized phonon states in an external magnetic field. *J. Phys. C Solid State Phys.* **9**, L297 (1976).

18. A. Spadoni, M. Ruzzene, S. Gonella, F. Scarpa, Phononic properties of hexagonal chiral lattices. *Wave Motion*. **46**, 435–450 (2009).

19. R. Süsstrunk, S. D. Huber, Observation of phononic helical edge states in a mechanical topological insulator. *Science*. **349**, 47–50 (2015).

20. C. Brendel, V. Peano, O. J. Painter, F. Marquardt, Pseudomagnetic fields for sound at the nanoscale. *Proc. Natl. Acad. Sci.* **114**, E3390–E3395 (2017).

21. T. Low *et al.*, Polaritons in layered two-dimensional materials. *Nat. Mater.* **16**, 182 (2017).
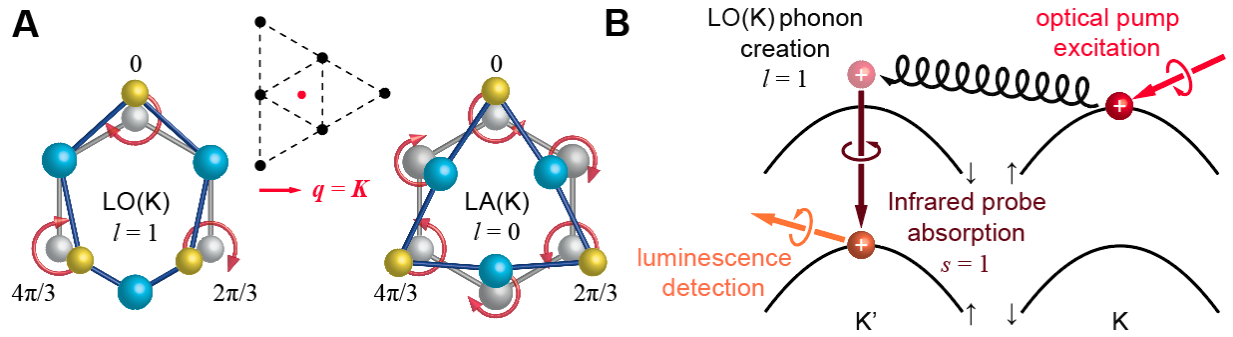
22. F. Ceballos, Q. Cui, M. Z. Bellus, H. Zhao, Exciton formation in monolayer transition metal dichalcogenides. *Nanoscale*. **8**, 11681–11688 (2016).

23. P. Steinleitner *et al.*, Direct Observation of Ultrafast Exciton Formation in a Monolayer of WSe2. *Nano Lett.* **17**, 1455–1460 (2017).

24. M. Manca *et al.*, Enabling valley selective exciton scattering in monolayer WSe$_2$ through upconversion. *Nat. Commun.* **8**, ncomms14927 (2017).

25. T. Yu, M. W. Wu, Valley depolarization due to intervalley and intravalley electron-hole exchange interactions in monolayer MoS2. *Phys. Rev. B*. **89**, 205303 (2014).

26. T. Yan, J. Ye, X. Qiao, P. Tan, X. Zhang, Exciton valley dynamics in monolayer WSe2 probed by the two-color ultrafast Kerr rotation. *Phys. Chem. Chem. Phys.* **19**, 3176–3181 (2017).

27. C. Poellmann *et al.*, Resonant internal quantum transitions and femtosecond radiative decay of excitons in monolayer WSe2. *Nat. Mater.* **14**, 889–893 (2015).

28. X.-X. Zhang *et al.*, Magnetic brightening and control of dark excitons in monolayer WSe2. *Nat. Nanotechnol.* **12**, 883–888 (2017).

29. M. M. H. Barreira, C. Wotzasek, Chiral-boson quantum mechanics. *Phys. Rev. D*. **45**, 1410–1415 (1992).

30. N. Li *et al.*, Colloquium: Phononics: Manipulating heat flow with electronic analogs and beyond. *Rev. Mod. Phys.* **84**, 1045–1066 (2012).

31. C. R. Zhu *et al.*, Exciton valley dynamics probed by Kerr rotation in WSe2 monolayers. *Phys. Rev. B*. **90**, 161302 (2014).

32. W.-T. Hsu *et al.*, Optically initialized robust valley-polarized holes in monolayer WSe2. *Nat. Commun.* **6**, 8963 (2015).

33. R. Braunstein, Intervalence band transitions in gallium arsenide. *J. Phys. Chem. Solids*. **8**, 280–282 (1959).

34. R. James, Direct free-hole absorption induced in germanium by 1.06 μm picosecond pulses. *IEEE J. Quantum Electron.* **19**, 701–710 (1983).

35. A. Chernikov, C. Ruppert, H. M. Hill, A. F. Rigosi, T. F. Heinz, Population inversion and giant bandgap renormalization in atomically thin WS2 layers. *Nat. Photonics*. **9**, 466–470 (2015).

36. A. S. Bolgar, Z. A. Trofimova, A. A. Yanaki, Thermodynamic properties of tungsten diselenide in a broad temperature range. *Sov. Powder Metall. Met. Ceram.* **29**, 382–385 (1990).

37. M. J. Rosker, M. Dantus, A. H. Zewail, Femtosecond real-time probing of reactions. I. The technique. *J. Chem. Phys.* **89**, 6113–6127 (1988).

38. X. Li *et al.*, Intrinsic electrical transport properties of monolayer silicene and MoS2 from first principles. *Phys. Rev. B*. **87**, 115418 (2013).

39. Z. Jin, X. Li, J. T. Mullen, K. W. Kim, Intrinsic transport properties of electrons and holes in monolayer transition-metal dichalcogenides. *Phys. Rev. B*. **90**, 045422 (2014).

40. D. K. Ferry, First-order optical and intervalley scattering in semiconductors. *Phys. Rev. B*. **14**, 1605–1609 (1976).

41. M. A. Pimenta *et al.*, Studying disorder in graphite-based systems by Raman spectroscopy. *Phys. Chem. Chem. Phys.* **9**, 1276–1290 (2007).

42. S. Mignuzzi *et al.*, Effect of disorder on Raman scattering of single-layer MoS2. *Phys. Rev. B*. **91**, 195411 (2015).

43. Z. Y. Zhu, Y. C. Cheng, U. Schwingenschlögl, Giant spin-orbit-induced spin splitting in two-dimensional transition-metal dichalcogenide semiconductors. *Phys. Rev. B*. **84**, 153402 (2011).

44. Y. Li *et al.*, Measurement of the optical dielectric function of monolayer transition-metal dichalcogenides: MoS2, MoSe2, WS2, and WSe2. *Phys. Rev. B*. **90**, 205422 (2014).

45. D. Le *et al.*, Spin–orbit coupling in the band structure of monolayer WSe2. *J. Phys. Condens. Matter*. **27**, 182201 (2015).

46. G. Wang *et al.*, Giant Enhancement of the Optical Second-Harmonic Emission of WSe2 Monolayers by Laser Excitation at Exciton Resonances. *Phys. Rev. Lett.* **114**, 097403 (2015).

Acknowledgements:

Fig. 1: Non-degenerate chiral phonons in monolayer WSe₂ and the selection rule of hole-phonon interactions. (A) The atomic motion of W and Se atoms (blue and yellow spheres) in the real space is intrinsically circular for the chiral phonons residing at the K point (red dot) in the reciprocal lattice (array of black dots), due to the three-fold rotational symmetry. Since the momentum vector determines the relative phase of the Se motion, opposite rotations correspond to completely different modes. The two modes have distinct PAM with respect to the center of the hexagon. **(B)** In the intervalley optical transition of holes, the PAM of the K-phonon is equal to the spin of the infrared photon due to angular momentum conservation. A hole injected by the left-circular-polarized optical pump moves from K to K' valley through virtual scattering with LO(K) phonon. Due to the spin and energy mismatch, a real phonon is created only if the hole simultaneously absorbs an infrared probe photon and transits to the spin-split state, which is signaled by the right-circular-polarized luminescence.
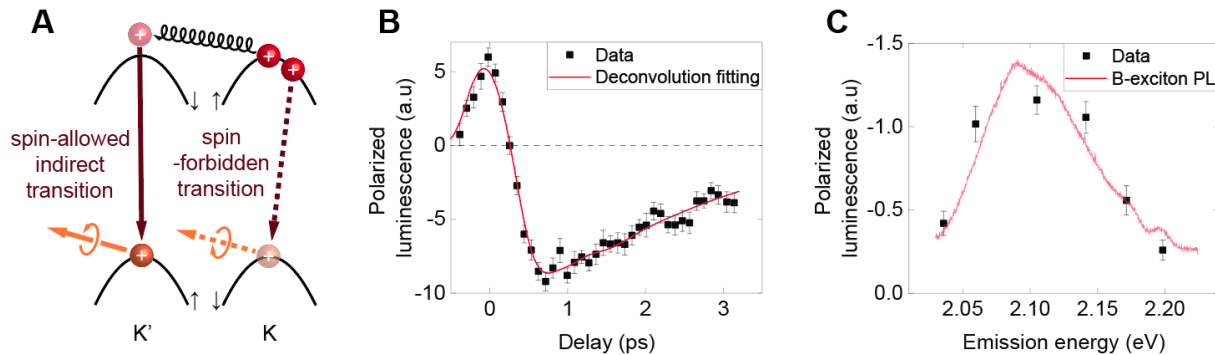
Fig. 2: Chiral phonon creation from the intervalley transition of holes measured by polarized luminescence. (A) The spin-allowed intervalley transition of holes from K point creates a K phonon, yet the spin-forbidden transition within the same valley does not. The two processes are distinguished by the polarized luminescence signal. **(B)** The observed initial positive polarization indicates spin-flipping transition of non-equilibrium holes, with a lifetime about 0.2 ps. After that the negative polarization shows prevailing phonon-creating intervalley transition of for valley-polarized holes, with a lifetime about 2 ps at 82 K. The pump and probe energy are tuned to 1.97 eV and 0.51 eV respectively, while the signal is integrated from 2.05 to 2.19 eV. **(C)** The spectrum of the polarized luminescence taken at $\tau = 0.8$ ps agrees with the B-exciton photoluminescence and confirms its spin-split-hole origin. The error bars are standard error calculated from multiple measurements.
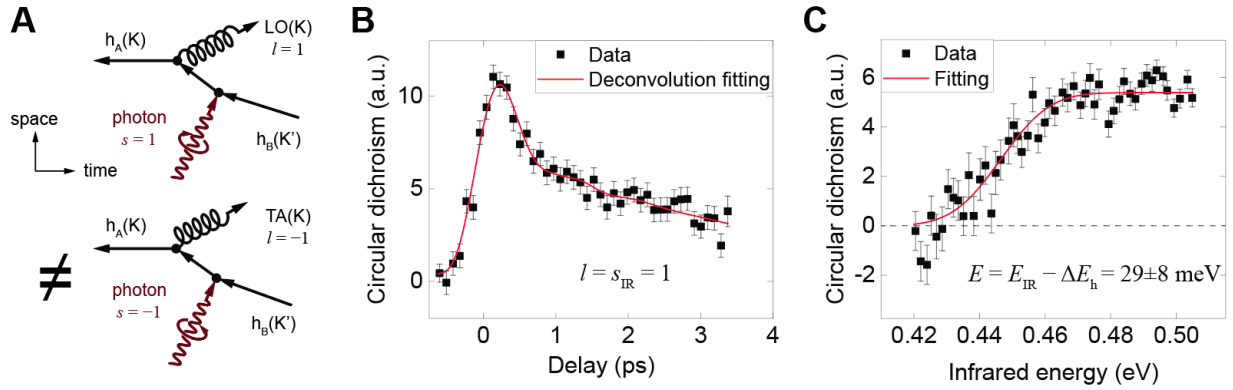
Fig. 3: Chirality of phonon measured by transient infrared circular dichroism (CD). (A) The phonons participating the indirect optical transition are different for the left- and right-circular-polarized IR photons because of the conservation of linear and angular momentum. Their distinct electron-phonon scattering strength dictates that the two processes have different amplitudes, leading to polarized IR absorption. **(B)** The measured CD at 82 K (black squares and red fitting curve) is positive for both the initial intravalley spin-flipping transition and the later intervalley phonon-creating transition. It not only proves the chirality of phonons but also means the LO phonon process is dominant. **(C)** The spectrum of the transient CD acquired at $\tau = 0.8$ ps shows a photonic energy threshold of 0.448±0.002 eV. Its step-shape is expected from the two-dimensional excitonic density of states. Subtracting the energy difference between the initial and final hole states, a phonon energy of 29±8 meV is deduced, agreeing with that of the LO mode. The error bars are standard error calculated from multiple measurements, and the threshold uncertainty is the standard error of the fitting parameter.

Supplementary Materials:

Materials and Methods

Figures S1-S12

Tables S1

Movies S1-S2

References (*31–46*)